

Mechanical and electrical fields of piezoelectric curved sensors

E. ARSLAN, R. USTA

*Department of Mechanical Engineering
Inonu University
Malatya, Turkey
e-mails: eray.arслан@inonu.edu.tr, usta_raif@hotmail.com*

BASED ON THE THEORY OF ELASTICITY, a comprehensive mathematical model is developed for a piezoelectric bimorph curved bar which is in a closed electrical circuit. First, the model is verified by considering an actuator under an initial electric potential, and the numerical results are compared with those of a related study in the literature. Then, the model is used to obtain the mechanical and electrical fields of a bimorph curved sensor subjected to a couple at its free end section. Hence, the bending that causes the generation of electric potential in the sensor is investigated. The influence of the applied couple on the mechanical and electrical fields in the curved sensor is examined, and the results are presented in graphical form.

Key words: piezoelectric materials, curved bimorph sensor and actuator, analytical model, bending moment.

Copyright © 2014 by IPPT PAN

1. Introduction

PIEZOELECTRIC MATERIALS ARE USED EXTENSIVELY in microengineering applications as either actuators or sensors [1]. In reversible sensor behavior, electric potential is generated in a material that is subjected to a mechanical load (direct effect). However, a piezoelectric material is considered to be actuator since displacement occurs in response to the application of an initial electric potential (converse effect) [2]. Generally, the material may be placed on a cantilever [2–4] or a curved elastic beam [5], depending on the purpose of its use. However, if a flat piezoelectric material is bonded onto structures that have complex shapes and uneven surfaces, the sensitivity of the material decreases [2]. Moreover, flat and curved materials exhibit totally different mechanical and electrical behaviors under load [6]. Hence, such behaviors of piezoelectric curved sensors and actuators should be examined in detail [6].

Bimorph [7–9] and multimorph [10, 11] piezoelectric cantilever sensors and actuators have been investigated by several researchers. In such investigations, while the actuators are considered to be subjected to an initial electric potential, the sensors are under bending moment or shear force. Moreover, mathematical models to describe the deformation and electrical behaviors also have been devel-

oped for functionally graded piezoelectric cantilever sensors [12–14] and actuators [13, 15]. In these studies, piezoelectric coefficients are assumed to vary in the radial direction according to some mathematical functions, such as polynomials, exponentials, or according to the power laws. On the other hand, there also are investigations in which curved actuators are taken into consideration. SHI [6] presented analytical models to describe the bending behavior of both bimorph and graded curved piezoelectric actuators. Shi assumed that the actuators, which are poled in the radial direction, are subjected to an electric potential between the inner and outer surfaces. SHI and ZHANG performed a similar analysis in which the piezoelectric coefficients are assumed to vary in the radial direction according to a Taylor series expansion [16] and to a second-order polynomial [17] for a curved actuator under external electric potential. However, there is no adequate analysis for a piezoelectric curved sensor subjected to mechanical loads in the literature. In order to fill this gap in the literature, the aim of the present work is to investigate the behavior of such a sensor subjected to a couple, which causes pure bending, as a mechanical load.

The purpose of the present study is to develop an analytical solution for a piezoelectric bimorph curved bar that is more comprehensive than Shi's model [6] and to present numerical results for a bimorph curved sensor under pure bending. The basic equations of the theory of elasticity for a cylindrical coordinate system have been used to derive the model [18–21]. First, the model is solved for a bimorph actuator for which an initial electric potential (closed circuit voltage) is applied to the outer surface, and the results are compared with those of Shi's model [6]. Then, the model is used to obtain the mechanical and electrical fields of a bimorph curved sensor subjected to a couple at its free end section. The influences of the applied couple on stresses, displacements, and electric potential have been investigated.

2. Basic equations

The geometry of the bimorph piezoelectric curved bar is presented in Fig. 1. The bar is considered in a closed electrical circuit [8, 9]. A cylindrical coordinate system (r, θ, z) is used in the entire analysis. It is assumed that both layers of the curved bar are polarized along the radial direction r and the direction of polarization is shown with an arrow in Fig. 1 [22]. It is also presumed that the two layers of the bar are perfectly joined together. This means that no sliding occurs on the interface surface between the layers under load. Further, it is assumed that a state of plane stress exists (axial stress components $\sigma_z^i = 0$) and small deformations are presumed. Here, and in the following equations, script i denotes the first or second layer of the bar ($i = I, II$). Because of the cylindrical symmetry assumption, only radial u and circumferential displacements v depend

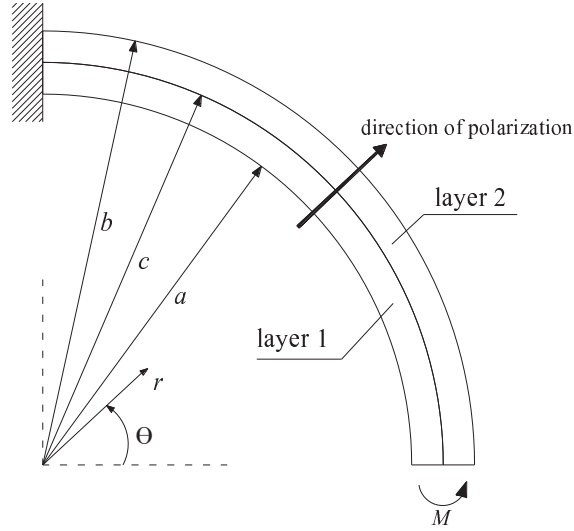


FIG. 1. Geometry of piezoelectric bimorph curved bar on which electrodes are located on the surfaces $r = a$ and $r = b$.

on circumferential coordinate θ but other quantities are only a function of radial coordinate r . Furthermore, this assumption requires that the shear stress $\tau_{r\theta}^i$, the shear strain $\gamma_{r\theta}^i$, the circumferential component of electric displacement vector D_θ^i , and circumferential electric field E_θ^i vanish. The governing constitutive equations are

$$(2.1) \quad \varepsilon_\theta^i = S_{11}\sigma_\theta^i + S_{13}\sigma_r^i + g_{31i}D_r^i,$$

$$(2.2) \quad \varepsilon_r^i = S_{13}\sigma_\theta^i + S_{33}\sigma_r^i + g_{33}D_r^i,$$

$$(2.3) \quad E_r^i = -g_{31i}\sigma_\theta^i - g_{33}\sigma_r^i + \zeta_{33}D_r^i,$$

where ε_j^i denote strains, σ_j^i are stresses, D_r^i are radial electric displacement vectors, S_{ij} are the components of the effective elastic compliance, g_{31i} and g_{33} are piezoelectric coefficients, and ζ_{33} is the dielectric permittivity coefficient. It should be emphasized that, although the piezoelectric coefficients (Type- g) g_{31i} are assumed to be different in the two layers, the other coefficients (i.e., S_{11} , S_{13} , S_{33} , g_{33} , and ζ_{33}) are the same in both layers since the dependence of g_{31i} on the degree of polling is more pronounced than those of the remaining coefficients [14]. The geometric relations read

$$(2.4) \quad \varepsilon_r^i = \frac{\partial u^i}{\partial r},$$

$$(2.5) \quad \varepsilon_\theta^i = \frac{u^i}{r} + \frac{1}{r} \frac{\partial v^i}{\partial \theta},$$

$$(2.6) \quad \gamma_{r\theta}^i = \frac{1}{r} \frac{\partial u^i}{\partial \theta} + \frac{\partial v^i}{\partial r} - \frac{v^i}{r} = 0.$$

Furthermore, the relationship between the radial electric field E_r^i and the electric potential ϕ^i requires

$$(2.7) \quad E_r^i = -\frac{d\phi^i}{dr}.$$

The compatibility equation is

$$(2.8) \quad \frac{d^2 \varepsilon_\theta^i}{dr^2} + \frac{2}{r} \frac{d\varepsilon_\theta^i}{dr} - \frac{1}{r} \frac{d\varepsilon_r^i}{dr} = 0.$$

Integrating the compatibility relation (2.8) by parts one finds [20]

$$(2.9) \quad \frac{d}{dr} (r\varepsilon_\theta^i) - \varepsilon_r^i = C_{2i},$$

where C_{2i} are arbitrary integration constants. The equations of equilibrium for the principal stresses and electric displacement vectors, in the absence of body force and body charge, may be expressed as

$$(2.10) \quad \frac{d\sigma_r^i}{dr} + \frac{\sigma_r^i - \sigma_\theta^i}{r} = 0,$$

$$(2.11) \quad \frac{1}{r} \frac{d}{dr} (rD_r^i) = 0.$$

3. Governing equations

Solution of Eq. (2.11) gives

$$(3.1) \quad D_r^i = \frac{C_{1i}}{r},$$

where C_{1i} are constants of integration. Keeping Eq. (2.10) in mind and substituting Eqs. (2.1), (2.2), and (3.1) into Eq. (2.9) give

$$(3.2) \quad r^2 S_{11} \frac{d^2 \sigma_r^i}{dr^2} + 3r S_{11} \frac{d\sigma_r^i}{dr} + (S_{11} - S_{33}) \sigma_r^i = \frac{C_{1i} g_{33}}{r} + C_{2i},$$

with the solution

$$(3.3) \quad \sigma_r^i = -\frac{C_{1i} g_{33}}{S_{33} r} + \frac{C_{2i}}{S_{11} - S_{33}} + C_{3i} r^{-1-S} + C_{4i} r^{-1+S},$$

where C_{3i} and C_{4i} are new integration constants and

$$(3.4) \quad S = \sqrt{\frac{S_{33}}{S_{11}}}.$$

From Eq. (2.10), the circumferential stress component is obtained as

$$(3.5) \quad \sigma_{\theta}^i = \frac{C_{2i}}{S_{11} - S_{33}} - C_{3i} S r^{-1-S} + C_{4i} S r^{-1+S}.$$

Equations (2.7), (3.1), (3.3), and (3.5) are put into Eq. (2.3) and then solved to obtain electric potential ϕ for layer i :

$$(3.6) \quad \phi^i = -C_{1i} \ln r \left(\zeta_{33} + \frac{g_{33}^2}{S_{33}} \right) + C_{2i} r \frac{(g_{31i} + g_{33})}{S_{11} - S_{33}} \\ - C_{3i} r^{-S} \frac{(g_{33} - g_{31i} S)}{S} + C_{4i} r^S \frac{(g_{33} + g_{31i} S)}{S} + C_{5i}.$$

At this point, new integration constants C_{5i} are introduced. For the derivation of the radial and circumferential displacements, the formulation in Timoshenko and Goodier [18] is used. Substituting the expressions above into relation (2.4) and integrating with respect to r , one obtains

$$(3.7) \quad u^i = \frac{C_{2i} r (S_{13} + S_{33})}{S_{11} - S_{33}} + \frac{C_{3i} r^{-S} (S S_{13} - S_{33})}{S} + \frac{C_{4i} r^S (S S_{13} + S_{33})}{S} + f_1^i,$$

where f_1^i are functions of θ only. Equation (2.5) can be expressed as

$$(3.8) \quad \varepsilon_{\theta}^i r - u^i = \frac{\partial v^i}{\partial \theta}.$$

Substituting Eqs. (2.1) and (3.7) into Eq. (3.8) and integrating for θ gives

$$(3.9) \quad v^i = \left\{ C_{1i} \left(g_{31i} - \frac{g_{33} S_{13}}{S_{33}} \right) \right. \\ \left. + \frac{r^{-S} [C_{2i} r^{1+S} S + (C_{3i} - C_{4i} r^{2S}) (S_{33} - S^2 S_{11})]}{S} \right\} \theta - \int f_1^i d\theta + f_2^i,$$

where f_2^i is a function that depends only on r . Thus, f_1^i and f_2^i can be obtained by substituting Eqs. (3.7) and (3.9) into Eq. (2.6):

$$(3.10) \quad f_1^i = \frac{C_{1i} (g_{31i} S_{33} - g_{33} S_{13})}{S_{33}} + D_{2i} \cos \theta + D_{3i} \sin \theta,$$

$$(3.11) \quad f_2^i = r D_{1i}.$$

Here, D_{1i} , D_{2i} , and D_{3i} are constants of integrations. Hence,

$$(3.12) \quad u^i = C_{1i} \left(g_{31i} - \frac{g_{33} S_{13}}{S_{33}} \right) + C_{2i} r \frac{(S_{13} + S_{33})}{S_{11} - S_{33}} + C_{3i} r^{-S} \frac{(S S_{13} - S_{33})}{S} \\ + C_{4i} r^S \frac{(S S_{13} + S_{33})}{S} + D_{2i} \cos \theta + D_{3i} \sin \theta,$$

$$(3.13) \quad v^i = r (D_{1i} + C_{2i} \theta) - D_{2i} \sin \theta + D_{3i} \cos \theta.$$

4. Solution for a bimorph piezoelectric curved sensor

To obtain a solution for the bimorph piezoelectric curved sensor, 16 unknown constants (i.e., C_{ji} and D_{ki} , where $i = 1, 2$; $j = 1, \dots, 5$; $k = 1, 2, 3$) should be calculated by using boundary and interface conditions. First, the following interface (mechanical and electrical) conditions are taken into account (for details see [6]):

$$(4.1) \quad D_r^I|_{r=c} = D_r^{II}|_{r=c},$$

$$(4.2) \quad \left. \frac{\partial u^I}{\partial \theta} \right|_{r=c, \theta=\frac{\pi}{2}} = \left. \frac{\partial u^{II}}{\partial \theta} \right|_{r=c, \theta=\frac{\pi}{2}} = 0,$$

to obtain

$$(4.3) \quad C_{11} = C_{12} = C_1,$$

$$(4.4) \quad D_{21} = D_{22} = 0,$$

Besides, as the interface conditions of the displacement components are used

$$(4.5) \quad u^I|_{r=c} = u^{II}|_{r=c},$$

$$(4.6) \quad v^I|_{r=c} = v^{II}|_{r=c},$$

the following relations are achieved:

$$(4.7) \quad D_{11} = D_{12} = D_1,$$

$$(4.8) \quad D_{31} = D_{32} = D_3.$$

$$(4.9) \quad C_{21} = C_{22} = C_2.$$

Furthermore, Eq. (4.5) also leads to the equality below [6]:

$$(4.10) \quad C_{19}g_{311} + C_{31}c^{-S} \frac{(SS_{13} - S_{33})}{S} + C_{41}c^S \frac{(SS_{13} + S_{33})}{S} \\ = C_{19}g_{312} + C_{32}c^{-S} \frac{(SS_{13} - S_{33})}{S} + C_{42}c^S \frac{(SS_{13} + S_{33})}{S}.$$

Hence, the number of undetermined constants has been decreased to 10 (i.e., C_i , C_{ji} , and D_k , where $i = 1, 2$; $j = 3, 4, 5$; $k = 1, 3$). For the determination of these constants, Eq. (4.10) and the following nine non-redundant boundary and interface conditions are used:

$$(4.11) \quad \phi^I|_{r=a} = 0,$$

$$(4.12) \quad \phi^{II}|_{r=b} = 0,$$

$$(4.13) \quad \sigma_r^I|_{r=a} = 0,$$

$$(4.14) \quad \sigma_r^{II}|_{r=b} = 0,$$

$$(4.15) \quad \phi^I|_{r=c} = \phi^{II}|_{r=c},$$

$$(4.16) \quad \sigma_r^I|_{r=c} = \sigma_r^{II}|_{r=c},$$

$$(4.17) \quad u^I|_{r=c, \theta=\frac{\pi}{2}} = 0,$$

$$(4.18) \quad v^I|_{r=c, \theta=\frac{\pi}{2}} = 0,$$

$$(4.19) \quad \int_a^c \sigma_\theta^I r dr + \int_c^b \sigma_\theta^{II} r dr = -M.$$

It should be noted that a necessary condition of

$$(4.20) \quad \int_a^c \sigma_\theta^I dr + \int_c^b \sigma_\theta^{II} dr = 0,$$

is automatically satisfied. Also note that the unknown constants are determined numerically.

5. Numerical results

In this section, first, the numerical results of the model for a curved actuator are verified by comparison with the results of Shi's study [6]. Then, the results of the model for the curved sensor are presented in graphical form. In all numerical results, we select the inner surface radius as $a = 16$ mm, the outer surface radius as $b = 17.32$ mm, and the interface radius as $c = 16.66$ mm (see Fig. 1) so that our results could be compared with Shi's results [6]. Furthermore, PZT-4 is considered to be a piezoelectric material in the treatment; then, the elastic coefficients are

$$S_{11} = 1.082 \times 10^{-11} \text{ m}^2/\text{N},$$

$$S_{13} = -2 \times 10^{-12} \text{ m}^2/\text{N},$$

$$S_{33} = 8.28 \times 10^{-12} \text{ m}^2/\text{N},$$

piezoelectric coefficients are

$$g_{311} = -12 \times 10^{-3} \text{ m}^2/\text{C},$$

$$g_{312} = 12 \times 10^{-3} \text{ m}^2/\text{C},$$

$$g_{33} = 2.6 \times 10^{-2} \text{ m}^2/\text{C},$$

and dielectric coefficient is $\zeta_{33} = 86.92 \times 10^6 \text{ m}/\text{F}$ [23].

5.1. Verification of the model

To verify the model, it is solved for a bimorph piezoelectric actuator, and the results are compared with those of Shi's solution [6]. To do so, the boundary conditions (4.12) and (4.19) are changed with

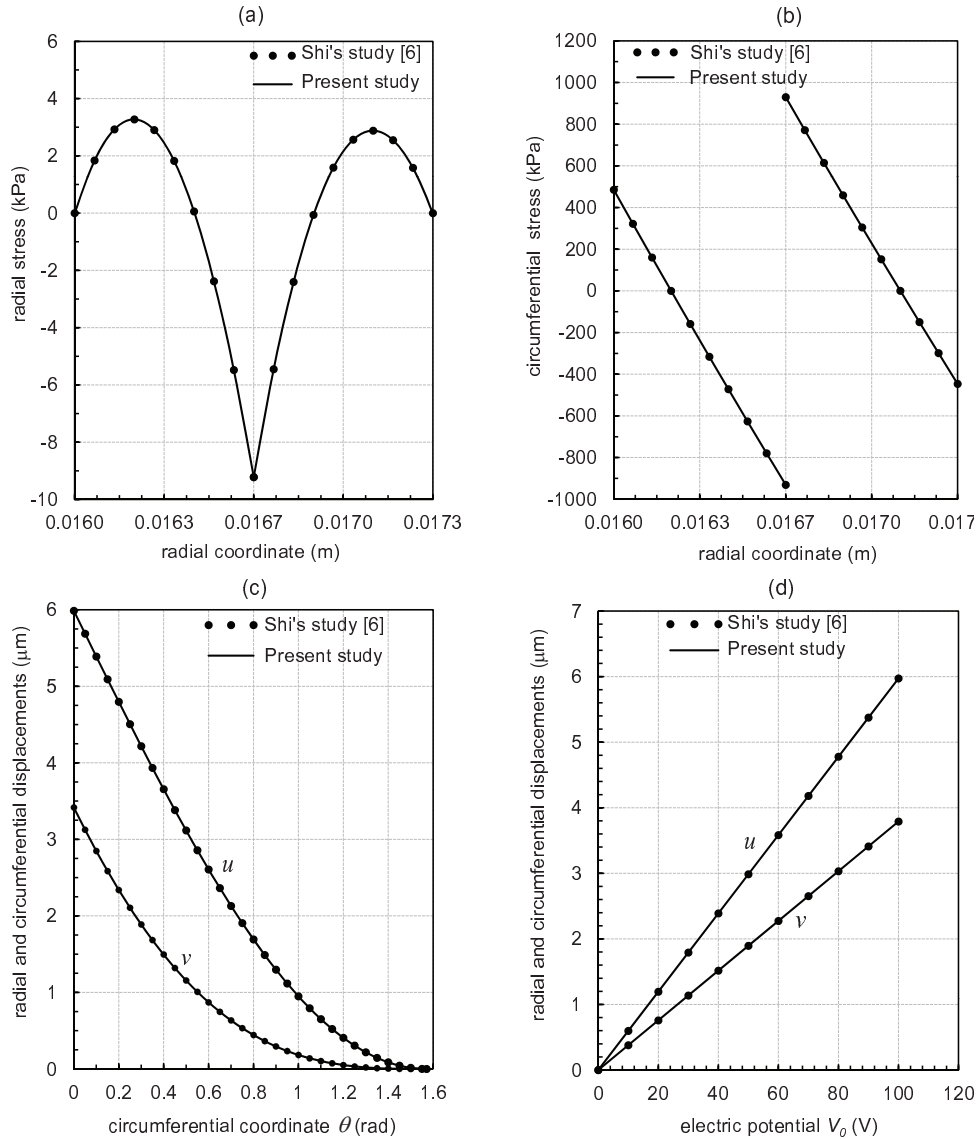


FIG. 2. Comparison of the response variables in the curved actuator obtained from the present study and those of Shi's solution [1]. The bar is subjected to excitation by a closed circuit electrical voltage ($V_0 = 100$ V), then, $\phi^I|_{r=a} = 0$ and $\phi^{II}|_{r=b} = V_0$.

$$(5.1) \quad \phi^{II}|_{r=b} = V_0,$$

$$(5.2) \quad \int_a^c \sigma_\theta^I r dr + \int_c^b \sigma_\theta^{II} r dr = 0,$$

while the other mechanical and electrical conditions remain the same as those in Section 4. Here, V_0 denotes an initial electric potential (closed circuit voltage) applied to the outer surface of the bar. Hence, the piezoelectric bar behaves as

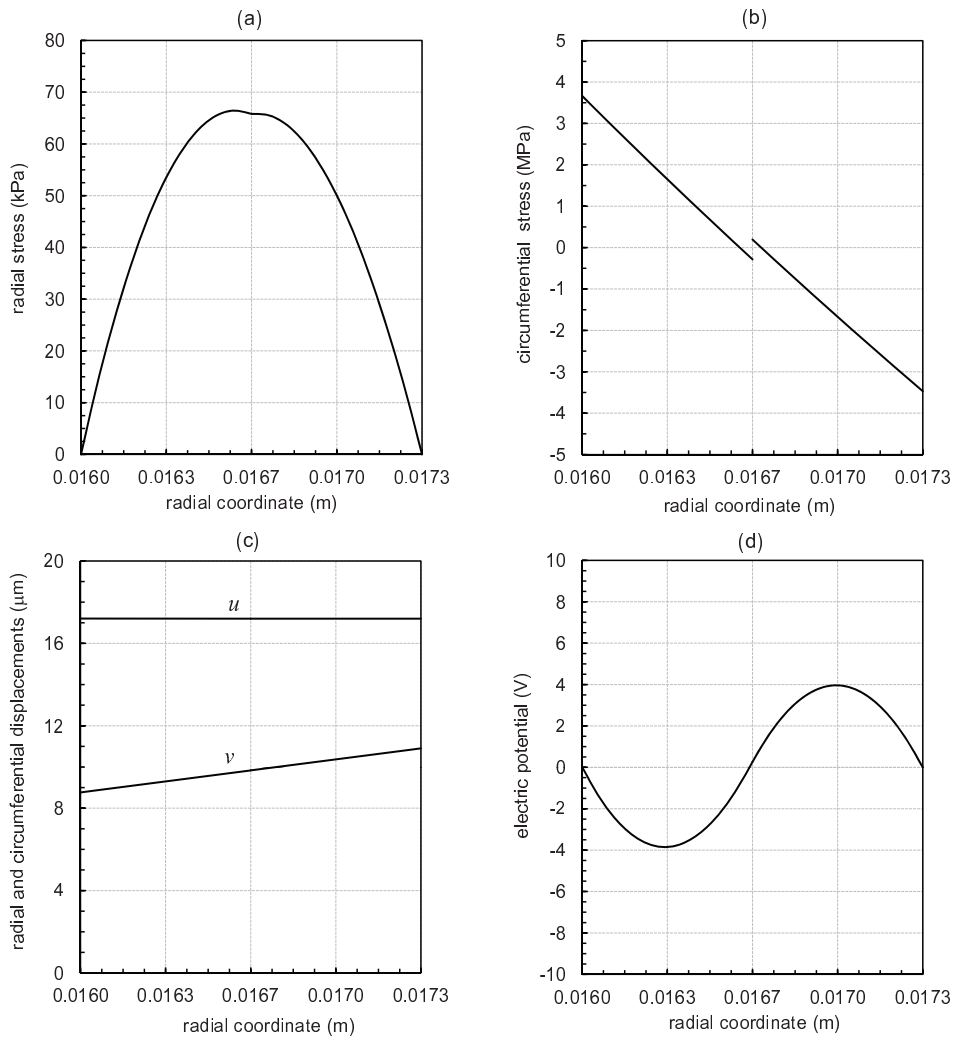


FIG. 3. Distributions of: a) radial stress, b) circumferential stress, c) displacements (at $\theta = 0$), d) electric potential in the radial coordinate r of the sensor on which $\phi^I|_{r=a} = 0$ and $\phi^{II}|_{r=b} = 0$ for $M = 1$ Nm.

an actuator, not a sensor. The numerical results of our model for the actuator and those of Shi's model [6] are compared in Fig. 2. Distributions of the radial and circumferential stresses in the radial coordinate and the displacements (at $r = c = 16.66$ mm) in the circumferential coordinate of the bimorph curved actuator are plotted in Figs. 2a–2c, respectively, for $V_0 = 100$ V. Furthermore, the changes in the radial and circumferential displacements at $r = c = 16.66$ mm with increasing initial electric potential V_0 (up to 100 V) are plotted in Fig. 2d. In each figure, the dots represent Shi's results [6], and the solid lines represent our model. The comparisons show that the solution provided by the present model agrees perfectly with that of Shi's model [6].

5.2. Results for the bimorph piezoelectric curved sensor

As discussed in the previous sections, as couple M is applied to the free end of the piezoelectric bar (see Fig. 1), it behaves as a sensor and produces electricity. The distributions of radial stress, circumferential stress, radial displacement, circumferential displacement, and electric potential on the radial coordinate of the curved sensor (with the dimensions given above) for $M = 1$ Nm are presented

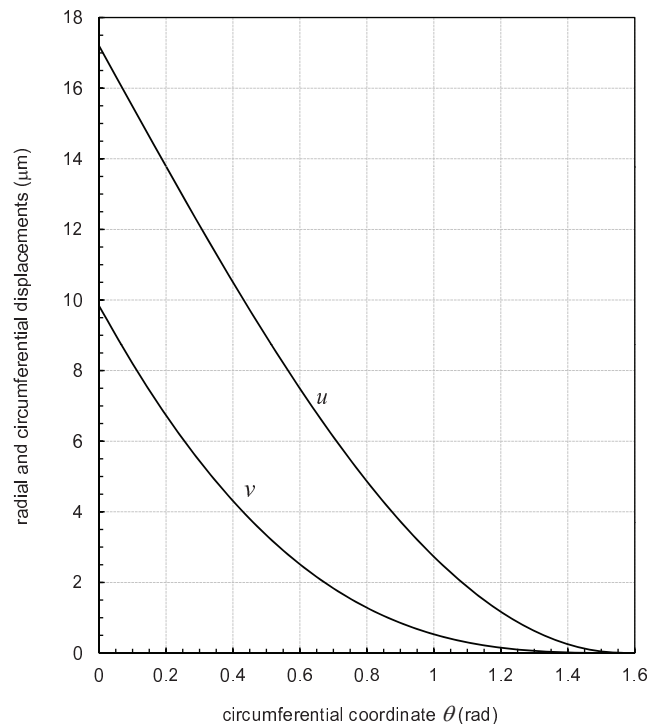


FIG. 4. Change in radial and circumferential displacements in the circumferential direction θ at $r = c = 0.01666$ m of the sensor for $M = 1$ Nm.

in Figs. 3a through 3d, respectively. It is important to remember that the electric potential is a function only of r but not θ (see Eq. (3.6)), and the distribution in the radial direction in Fig. 3d proves that an electrical potential difference, which may be called close circuit electrical voltage, occurs in the sensor in the radial direction under the specified load. In Fig. 3c, the displacement components are calculated for $\theta = 0$, which is the free end of the sensor. Under the same load, the changes in the radial and circumferential displacements in circumferential direction θ at constant interface radius ($r = c = 0.01666$ m) are plotted in Fig. 4.

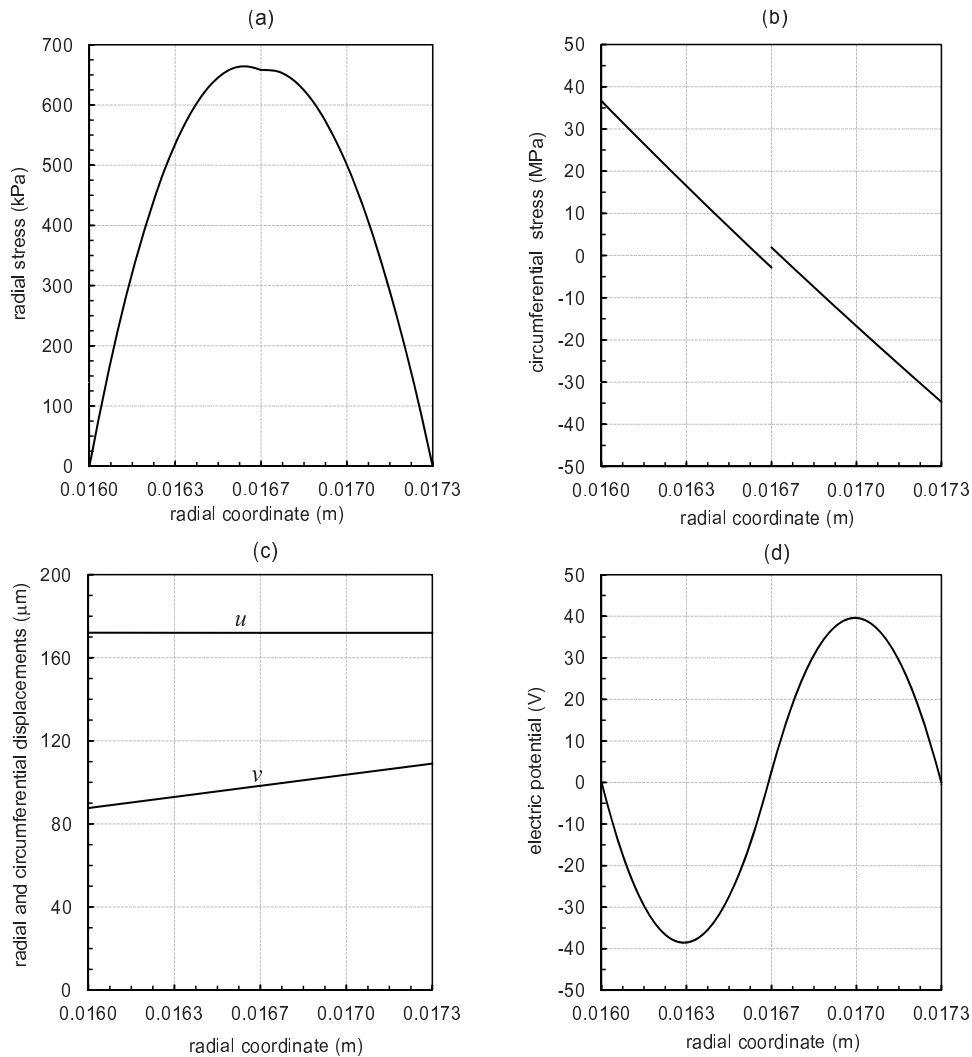


FIG. 5. Distributions of: a) radial stress, b) circumferential stress, c) displacements (at $\theta = 0$), and d) electric potential in the radial coordinate of the sensor on which $\phi^I|_{r=a} = 0$ and $\phi^{II}|_{r=b} = 0$ for $M = 10$ Nm.

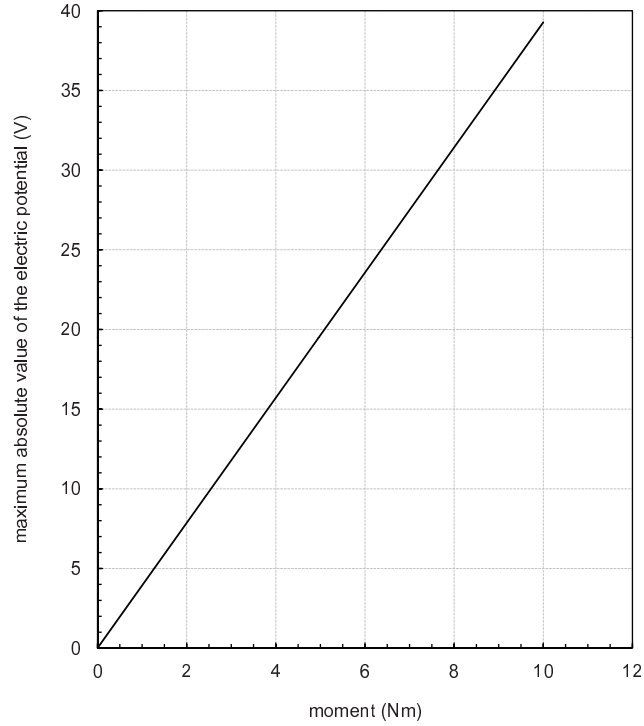


FIG. 6. Change in the maximum absolute value of the electric potential (V) generated across the bar $a \leq r \leq b$ on which $\phi^I|_{r=a} = 0$ and $\phi^{II}|_{r=b} = 0$, as M increases.

As seen in the figure, these infinitesimal deformation components decrease as θ approaches $\pi/2$, and they are equal to zero at the fixed end of the sensor (see also Fig. 1). The response variables for $M = 10$ Nm are presented in Fig. 5. It should be emphasized that, while the maximum absolute value of the electric potential generated in the sensor is around 3.96 V, which occurs on $r = 0.01698$ m for $M = 1$ Nm (see Fig. 3d), it is around 39.6 V at the same radial coordinate but for $M = 10$ Nm (see Fig. 5d). These results indicate that, when the couple is increased tenfold, the response variables also increase by the same rate. This observation proves that a linear relationship exists between the couple and the response variables. To simulate this relationship, the change in the maximum absolute value of the electric potential across the bar $a \leq r \leq b$ with increasing M is presented in Fig. 6.

6. Concluding remarks

Based on the theory of elasticity, an analytical model is presented for the mechanical and electrical fields of a piezoelectric bimorph curved bar which is in

a closed electrical circuit. The bar is considered first as an actuator by selecting the appropriate boundary conditions, and the accuracy of our model is verified by comparing our results with the results obtained Shi's model [6]. Hence, the boundary conditions are set to obtain a distribution of stresses, displacements, and electric potential in a bimorph curved sensor subjected to a couple at its free end, and numerical results are obtained for PZT-4. The results show that the electric potential generated in the sensor increased at the same rate as the applied moment. The model may be used for any curved actuators and sensors, depending on the boundary conditions with different dimensions. Hence, the model and the results may serve as a basis for producers who use piezoelectric materials bonded to complex structures with curved surfaces.

References

1. S. TADIGADAPA, K. MATETI, *Piezoelectric MEMS sensors: state-of-the-art and perspectives*, Measurement Science Technology, **20**, 092001, 2009.
2. P. KIELCZYNSKI, W. PAJEWSKI, M. SZALEWSKI, *Piezoelectric sensors for investigations of microstructures*, Sensors and Actuators A, **65**, 13–18, 1998.
3. M.H. SHEN, *Analysis of beams containing piezoelectric sensors and actuators*, Smart Material Structures, **3**, 439–447, 1994.
4. C. ONAT, M. SAHIN, Y. YAMAN, *Fractional controller design for suppressing smart beam vibrations*, Aircraft Engineering and Aerospace Technology: An International Journal, **84**, 203–212, 2012.
5. D. SUN, L. TONG, *Modeling and analysis of curved beams with debonded piezoelectric sensor/actuator patches*, International Journal of Mechanical Sciences, **44**, 1755–1777, 2002.
6. Z.F. SHI, *Bending behavior of piezoelectric curved actuator*, Smart Materials and Structures, **14**, 835–842, 2005.
7. J.G. SMITS, S.I. DALKE, T.K. COONEY, *The constituent equations of piezoelectric bimorphs*, Sensors and Actuators A, **28**, 41–61, 1991.
8. M. BRISSAUD, *Modelling of non-symmetric piezoelectric bimorphs*, Journal of Micromechanics and Microengineering, **14**, 1507–1518, 2004.
9. M. BRISSAUD, S. LEDREN, P. GONNARD, *Modelling of a cantilever non-symmetric piezoelectric bimorph*, Journal of Micromechanics and Microengineering, **13**, 832–844, 2003.
10. H.J. XIANG, Z.F. SHI, *Static analysis for multi-layered piezoelectric cantilevers*, International Journal of Solids and Structures, **45**, 113–128, 2008.
11. M.S. WEINBERG, *Working equations for piezoelectric actuators and sensors*, Journal of Microelectromechanical Systems, **8**, 529–533, 1999.
12. Z.F. SHI, Y. CHEN, *Functionally graded piezoelectric cantilever beam under load*, Archive of Applied Mechanics **74**, 237–247, 2004.
13. T. LIU, Z.F. SHI, *Bending behavior of functionally gradient piezoelectric cantilever*, Ferroelectrics, **308**, 43–51, 2004.

14. T. YU, Z. ZHONG, *Bending analysis of a functionally graded piezoelectric cantilever beam*, Science in China Series G: Physics, Mechanics & Astronomy, **50**, 97–108, 2007.
15. T. HAUKE, A. KOUVATOV, R. STEINHAUSEN, W. SEIFERT, H. BEIGE, H.T. LANGHAMMER, H.P. ABICHT, *Bending behavior of functionally gradient materials*, Ferroelectrics, **238**, 195–202, 2000.
16. Z.F. SHI, T. ZHANG, *Bending analysis of a piezoelectric curved actuator with a generally graded property for the piezoelectric parameter*, Smart Materials and Structures, **17**, 045018, 2008.
17. T. ZHANG, Z.F. SHI, *Two-dimensional exact analysis for piezoelectric curved actuators*, Journal of Micromechanics and Microengineering, **16**, 640–647, 2006.
18. S.P. TIMOSHENKO, J.N. GOODIER, *Theory of Elasticity*, McGraw-Hill, 1970.
19. E. ARSLAN, A.N. ERASLAN, *Bending of graded curved bars at elastic limits and beyond*, International Journal of Solids and Structures, **50**, 806–814, 2013.
20. E. ARSLAN, A.N. ERASLAN, *Analytical solution to the bending of a nonlinearly hardening wide curved bar*, Acta Mechanica, **210**, 71–84, 2010.
21. E. ARSLAN, I.Y. SULU, *Yielding of a two-layer curved bar under pure bending*, Zeitschrift für Angewandte Mathematik und Mechanik, **94**, 713–720, 2014.
22. P. KIELCZYNSKI, W. PAJEWSKI, *Influence of a layered polarization of piezoelectric ceramics on shear-horizontal surface-wave propagation*, Applied Physics B, **48**, 383–388, 1989.
23. X. RUAN, S.C. DANFORTH, A. SAFARI, T.W. CHOUA, *Saint-Venant end effects in piezoceramic materials*, International Journal of Solids and Structures, **37**, 2625–2637, 2000.

Received January 29, 2014; revised version May 13, 2014.
